Acta Cryst E CRYSTALLOGRAPHIC COMMUNICATIONS

ISSN 2056-9890

1-Ethyl 2-methyl 3,4-bis(acetyloxy)pyrrolidine-1,2-dicarboxylate: crystal structure, Hirshfeld surface analysis and computational chemistry

Sofia Dallasta Pedroso,[a] Ignez Caracelli,[b]* Julio Zukerman-Schpector,[a] Monica Soto-Monsalve,[c] Regina H. De Almeida Santos,[c] Carlos Roque D. Correia,[d] Ariel L. Llanes Garcia,[d] Huey Chong Kwong[e] and Edward R. T. Tiekink[e]‡

[a]Laboratório de Cristalografia, Esterodinâmica e Modelagem Molecular, Departamento de Química, Universidade Federal de São Carlos, 13565-905 São Carlos, SP, Brazil, [b]Departmento de Física, Universidade Federal de São Carlos, 13565-905 São Carlos, SP, Brazil, [c]Instituto de Química de São Carlos, Universidade de São Paulo, São Carlos, SP, Brazil, [d]Instituto de Química, Universidade Estadual de Campinas, UNICAMP, CP 6154, CEP 13084-917 Campinas, Brazil, and [e]Research Centre for Crystalline Materials, School of Science and Technology, Sunway University, 47500 Bandar Sunway, Selangor Darul Ehsan, Malaysia. *Correspondence e-mail: ignez@df.ufscar.br

Received 18 May 2020
Accepted 24 May 2020

Edited by W. T. A. Harrison, University of Aberdeen, Scotland

‡ Additional correspondence author, e-mail: edwardt@sunway.edu.my.

Keywords: crystal structure; pyrrolidine; Hirshfeld surface analysis; NCI plots; computational chemistry.

CCDC reference: 2005478

Supporting information: this article has supporting information at journals.iucr.org/e

The title compound, $C_{13}H_{19}NO_8$, is based on a tetra-substituted pyrrolidine ring, which has a twisted conformation about the central C—C bond; the $C_m—C_a—C_a—C_{me}$ torsion angle is 38.26 (15)° [m = methylcarboxylate, a = acetyloxy and me = methylene]. While the N-bound ethylcarboxylate group occupies an equatorial position, the remaining substituents occupy axial positions. In the crystal, supramolecular double-layers are formed by weak methyl- and methylene-C—H···O(carbonyl) interactions involving all four carbonyl-O atoms. The two-dimensional arrays stack along the *c* axis without directional interactions between them. The Hirshfeld surface is dominated by H···H (55.7%) and H···C/C···H (37.0%) contacts; H···H contacts are noted in the inter-double-layer region. The interaction energy calculations point to the importance of the dispersion energy term in the stabilization of the crystal.

1. Chemical context

A number of diseases, especially diabetes but also including viral diseases, cystic fibrosis and cancer, can be treated with α-glucosidase inhibitors (Dhameja & Gupta, 2019; Kiappes *et al.*, 2018); for a review of the relevant patent literature, see Brás *et al.* (2014). Imino- and aza-sugars are strong inhibitors of the enzyme and are attracting current interest for chaperone therapy of Gaucher disease (Matassini *et al.*, 2020). The tri-hydroxyl-substituted compound, aminociclitol, (I), is a known α-glucosidase inhibitor and is a natural product, being found in several plants (Assefa *et al.*, 2020). The synthesis of (I) can proceed from several key intermediates (Garcia, 2008; Liu & Ma, 2017) and it is this consideration that prompted the structural investigation of the title compound, $C_{13}H_{19}NO_8$, (II). Specifically, the HCl salt of (I) can be prepared from (II) after being subjected to a sequence of reactions comprising a reduction step, reflux acid hydrolysis, chromatographic purification on ion-exchange resin Dowex-H^+ and, finally, hydrochloride formation. In this way, (I)·HCl was obtained in 67% yield (Garcia, 2008). In connection with supporting structural studies (Zukerman-Schpector *et al.*, 2017) of crucial intermediates related to the synthesis of pharmacologically active (I), herein, the crystal and molecular structures of (II) are described. This is complemented by a detailed analysis of the

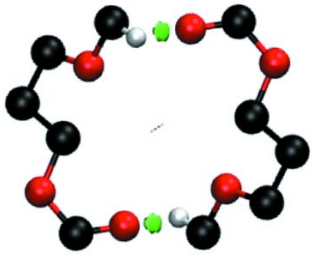

supramolecular architecture by Hirshfeld surface analysis, non-covalent interactions plots and computational chemistry.

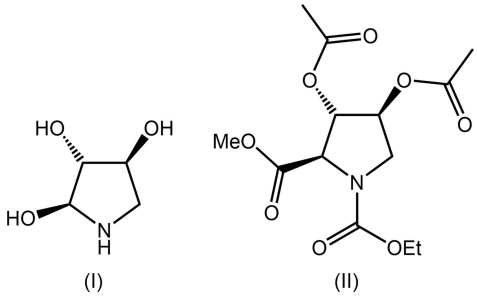

(I) (II)

2. Structural commentary

The molecular structure of (II), Fig. 1, features a tetra-substituted pyrrolidine ring. The conformation of the five-membered ring is best described as being twisted about the C2—C3 bond; the C1—C2—C3—C4 torsion angle is 38.26 (15)° indicating a (+)*syn*-clinal configuration. With respect to the five-membered ring, the *N*-bound methyl-carboxylate substituent occupies an equatorial position; the sum of angles about the N1 atom amounts to 360°, indicating this is an sp^2 centre. At the C1–C3 centres, the methyl-carboxylate and 2 × acetyloxy substituents, respectively, occupy axial positions. For the molecule illustrated in Fig. 1, the chirality of each of the C1–C3 atoms is *R*, *S* and *S*, respectively; the centrosymmetric unit cell contains equal numbers of each enantiomer. When viewed towards the approximate plane through the pyrrolidine ring, the N-bound substituent is approximately co-planar, the C2-acetyloxy lies to one side of the plane, and the C1- and C3-substituents lie to the other side.

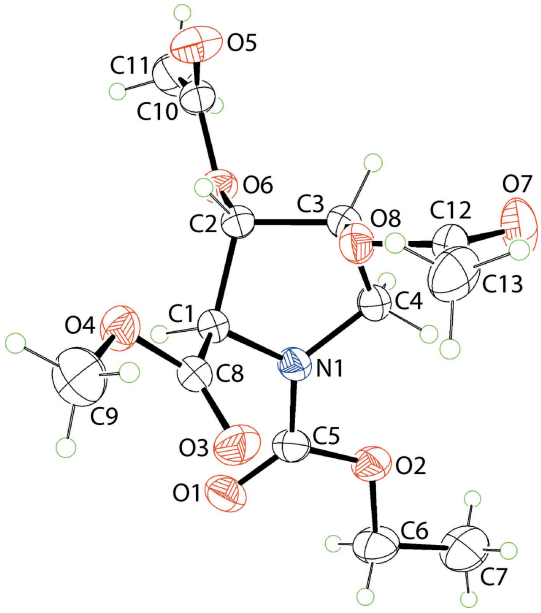

Figure 1
The molecular structure of (II), showing the atom-labelling scheme and displacement ellipsoids at the 35% probability level.

Table 1
Hydrogen-bond geometry (Å, °).

D—H···*A*	*D*—H	H···*A*	*D*···*A*	*D*—H···*A*
C9—H9*B*···O5^{i}	0.96	2.53	3.403 (3)	151
C3—H3···O1^{ii}	0.98	2.62	3.419 (2)	139
C3—H3···O3^{ii}	0.98	2.61	3.453 (2)	144
C11—H11*A*···O7^{iii}	0.96	2.66	3.329 (3)	127

Symmetry codes: (i) $-x, -y, -z+2$; (ii) $x-1, y, z$; (iii) $x, y-1, z$.

3. Supramolecular features

There are two classes of identifiable non-covalent C—H···O interactions occurring in the crystal of (II). As identified in *PLATON* (Spek, 2020), methyl-C9—H···O5(carbonyl) contacts (Table 1) occur between centrosymmetrically related molecules to form a dimeric aggregate and an 18-membered $\{\cdots OCOC_3OCH\}_2$ synthon, Fig. 2(*a*). The second level, *i.e.* weaker, of C—H···O interactions assemble molecules into a supramolecular layer in the *ab* plane, Fig. 2(*b*), at separations beyond normally accepted values in *PLATON* (Spek, 2020). Here, a methylene-C3—H atom is bifurcated, forming contacts with the carbonyl-O1 and O3 atoms of a translationally related molecule along the *a*-axis direction. This is complemented by a methyl-C11—H···O7(carbonyl) interaction occurring along the *b*-axis direction, Fig. 2(*c*). The layer thus formed by these contacts is connected into a double-layer *via* the methyl-C9—H···O5(carbonyl) interactions mentioned above. The double-layers stack along the *c* axis without directional interactions between them.

4. Non-covalent interaction plots

Before embarking on a more detailed analysis of the overall molecular packing of (II), in particular of the inter-layer region along the *c* axis, non-covalent interaction plots

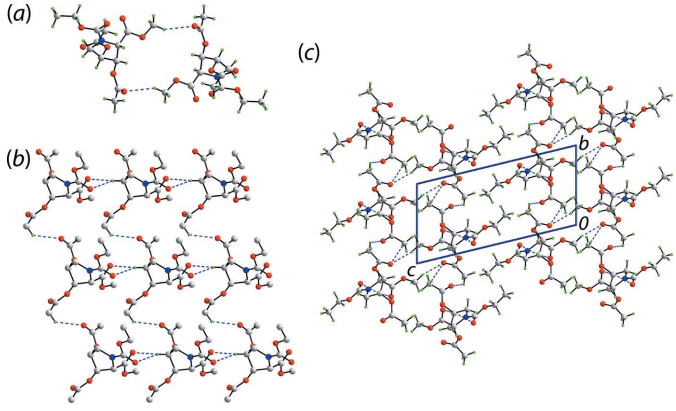

Figure 2
Molecular packing in (II): (*a*) supramolecular dimer sustained by methyl-C9—H···O5(carbonyl) contacts, (*b*) layer sustained by methyl-C11—H···O7(carbonyl) and bifurcated methylene-C3—H···O1,O3(carbonyl) contacts (non-participating H atoms are omitted) and (*c*) a view of the unit-cell contents shown in projection down the *a* axis. The C—H···O interactions are shown as blue dashed lines.

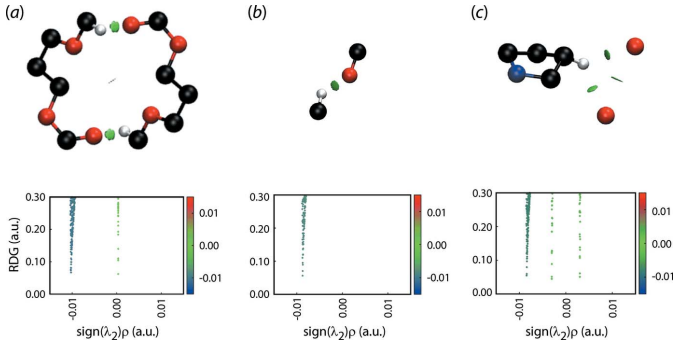

Figure 3
Non-covalent interaction plots for the following interactions in (II): (*a*) methyl-C9—H···O5(carbonyl), (b) methyl-C11—H···O7(carbonyl) and (c) bifurcated methylene-C3—H···O1,O3(carbonyl).

(Johnson *et al.*, 2010; Contreras-García *et al.*, 2011) were calculated to analyse in more detail the nature of the specified C—H···O contacts described in *Supramolecular features*. This method analyses the electron density (and derivatives) around the specified intermolecular contacts and generates colour-based isosurfaces as detailed in the cited literature. The results, through a three-colour scheme, enable the visualization of contacts as being attractive (blue isosurface), repulsive (red) or otherwise. For the weak interactions in focus, a green isosurface indicates a weakly attractive interaction.

The isosurfaces for three identified C—H···O contacts are given in the upper view of Fig. 3, and each displays a green isosurface indicating weakly attractive interactions. The lower views of Fig. 3 show the plots of RDG *versus* sign(λ^2)$\rho(r)$ for the three sets of C—H···O interactions. The green peaks apparent at density values less than 0.0 a.u. indicate these are weakly attractive interactions.

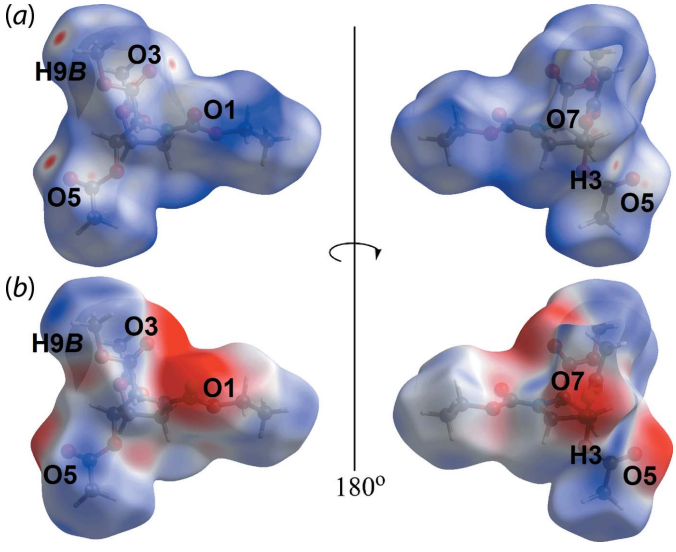

Figure 4
Two views of the Hirshfeld surface mapped for (II) over (*a*) d_{norm} in the range of −0.083 to +1.828 arbitrary units and (*b*) the calculated electrostatic potential in the range of −0.077 to 0.054 a.u.

5. Hirshfeld surface analysis

In order to understand further the interactions operating in the crystal of (II), the calculated Hirshfeld surfaces were mapped over the normalized contact distance, d_{norm} (McKinnon *et al.*, 2004) and electrostatic potential (Spackman *et al.*, 2008) with associated two-dimensional (2-D) (full and delineated) fingerprint (FP) plots (Spackman & McKinnon, 2002). These were generated using *Crystal Explorer 17* (Turner *et al.*, 2017) following literature procedures (Tan *et al.*, 2019). The potentials were calculated using the STO-3G basis set at the Hartree–Fock level of theory. The bright-red spots on the Hirshfeld surface mapped over d_{norm}, Fig. 4(*a*), near the carbonyl-O (O1, O3, O5 and O7) and methyl-C—H (H3 and H9*B*) atoms correspond to the C—H···O interactions listed in Table 1. These observations were confirmed through the Hirshfeld surface mapped over the calculated electrostatic potential in Fig. 4(*b*), where the surface around carbonyl-O and methyl-C—H atoms are shown in red (negative electrostatic potential) and blue (positive electrostatic potential), respectively. Besides the C—H···O interactions listed in Table 1, a long C13—H13*A*···O5 interaction is reflected in the d_{norm} surface as a faint red spot in Fig. 5(*a*). In addition, short,

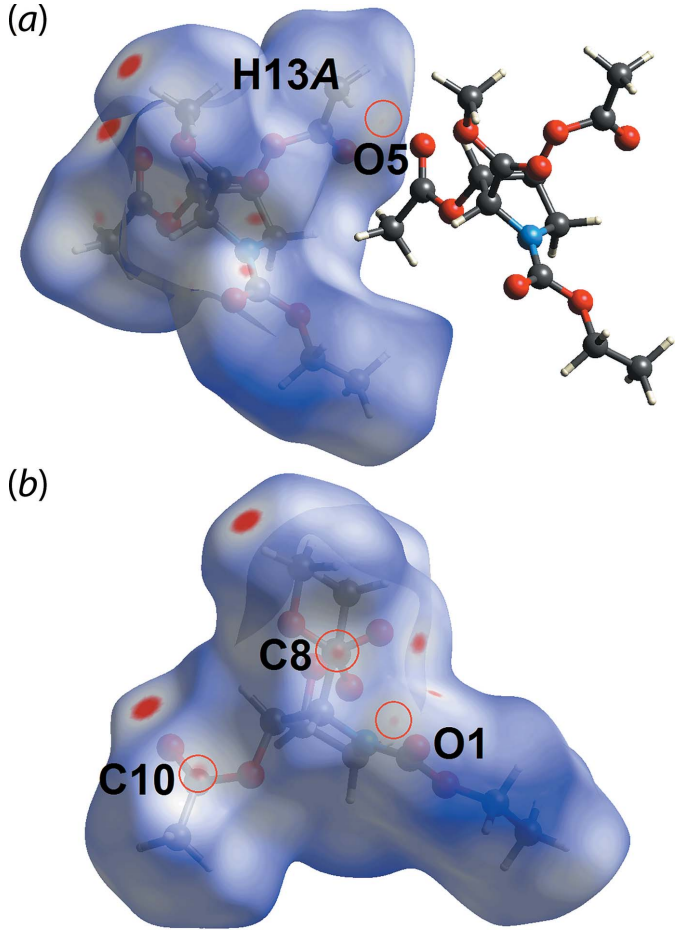

Figure 5
Views of the Hirshfeld surface mapped over d_{norm} for (II) in the range −0.083 to +1.828 arbitrary units, highlighting within red circles (*a*) a weak C—H···O interaction and (*b*) C···O contacts.

Table 2
Summary of short interatomic contacts (Å) in (I)[a].

Contact	Distance	Symmetry operation
H4*B*···H11*C*	2.32	$x+1, y+1, z$
H9*B*···O5[b]	2.42	$-x, -y, -z+2$
H3···O1[b]	2.55	$x-1, y, z$
H3···O3 [b]	2.53	$x-1, y, z$
H11*A*···O7[b]	2.59	$-x, -y+1, -z$
H13*A*···O5	2.58	$x+1, y+1, z$
C8···O5	3.191 (2)	$x+1, y, z$
C10···O1	3.204 (2)	$x-1, y, z$
C10···O7	3.185 (3)	$x, y-1, z$

Notes: (*a*) The interatomic distances are calculated in *Crystal Explorer 17* (Turner *et al.*, 2017) whereby the *X*—H bond lengths are adjusted to their neutron values. (*b*) These interactions correspond to the interaction listed in Table 1.

intra-layer C···O contacts with separations 0.01–0.04 Å shorter than the sum of their van der Waals radii, Table 2, are observed as faint red spots on the d_{norm} surface in Fig. 5(*b*), reflecting the specific influence of the C8, C10 and O1 atoms participating in these contacts.

The corresponding two-dimensional fingerprint plot for the Hirshfeld surface of (II) is shown with characteristic pseudo-symmetric wings in the upper left and lower right sides of the d_e and d_i diagonal axes, respectively, in Fig. 6(*a*). The individual H···H, H···O/O···H, H···C/C···H, O···O, O···C/C···O and H···N/N···H contacts are illustrated in the delineated two-dimensional fingerprint plots (FP) in Fig. 6(*b*)–(*g*), respectively; the percentage contributions from different interatomic contacts are summarized in Table 3. The H···H contacts contribute 55.7% to the overall Hirshfeld surface with a beak-shape distribution in the FP with shortest $d_e = d_i$ ~2.4 Å. This short interatomic H···H contact involving the methyl-H11*C* and methylene-H4*B* atoms, Table 2, is around the sum of their van der Waals separation and occurs in the intra-layer region along the *b* axis. Consistent with the C—H···O interactions making the major contribution to the directional interactions in the crystal, H···O/O···H contacts contribute 37.0% to the overall Hirshfeld surface. A distinctive feature in the FP of Fig. 6(*c*), is the two symmetric spikes at $d_e + d_i$ ~2.4 Å. Although H···C/C···H, O···O, O···C/C···O and H···N/N···H appear as splash-like distributions of points at $d_e + d_i$ ~3.0 Å, Fig. 6(*d*)–(*g*), their contributions to the overall Hirshfeld surface are each below than 3.0%. These contacts and the remaining interatomic contacts have only a small effect on the packing, as the sum of their contributions to the overall Hirshfeld surface is less than 8%.

6. Energy frameworks

The pairwise interaction energies between the molecules in the crystal of (II) were calculated using the wave function at the B3LYP/6-31G(d,p) level of theory. The total energy comprise four terms: electrostatic (E_{ele}), polarization (E_{pol}), dispersion (E_{dis}) and exchange-repulsion (E_{rep}) and were scaled as 1.057, 0.740, 0.871 and 0.618, respectively (Edwards *et al.*, 2017). The characteristics of the intermolecular interactions in term of their energies are collated in Table 4. In the

Table 3
Percentage contributions of interatomic contacts to the Hirshfeld surface for (II).

Contact	Percentage contribution
H···H	55.7
H···O/O···H	37.0
H···C/C···H	2.7
O···O	2.3
O···C/C···O	1.9
H···C/C···H	0.4

absence of conventional hydrogen bonding in the crystal, the dispersive component makes the major contribution to the interaction energies (Table 4). According to the total interaction energy, molecules within the supramolecular double layer are stabilized by C—H···O interaction, C···O short

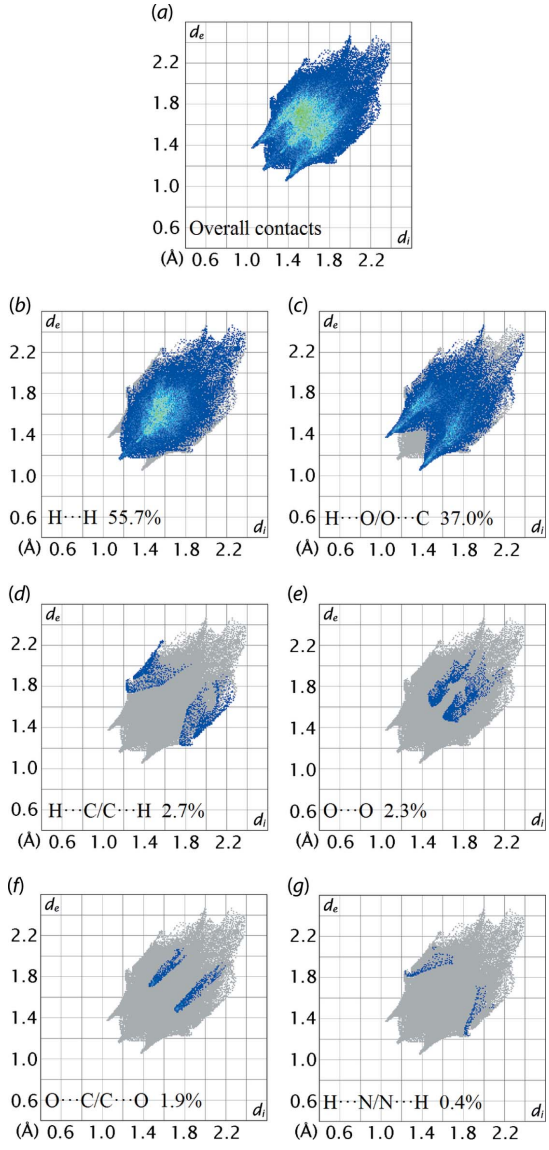

Figure 6
(*a*) The full two-dimensional fingerprint plot for (II) and (*b*)–(*g*) those delineated into H···H, O···H/H···O, C···H/H···C, O···O, C···O/O···C and H···N/N···H contacts, respectively.

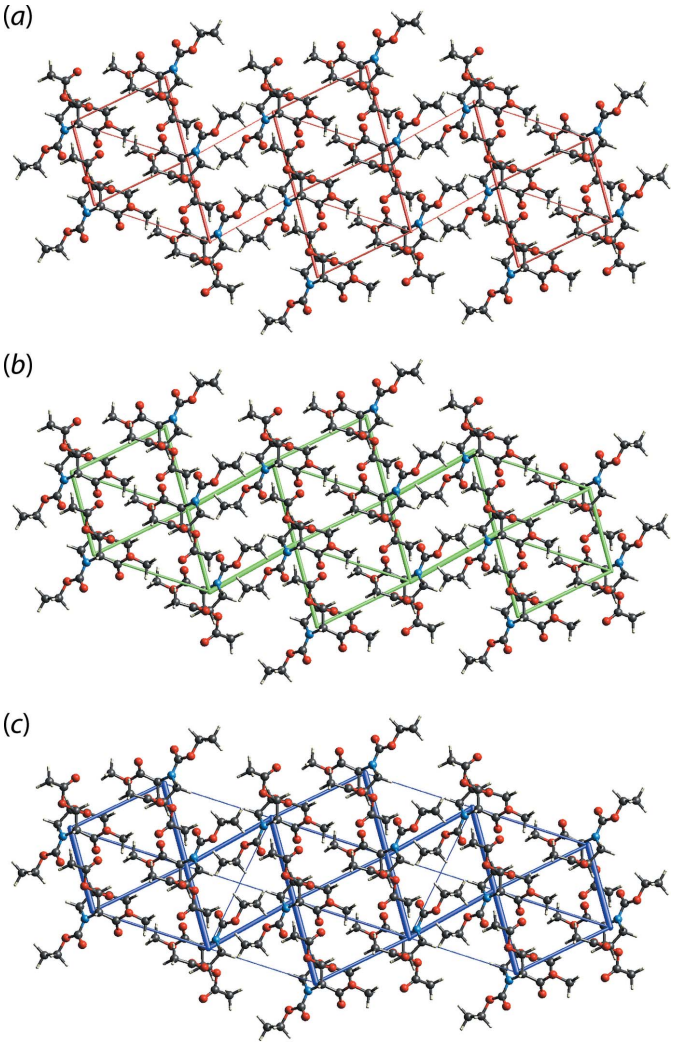

Figure 7
Perspective views of the energy frameworks calculated for (II) and viewed down the *b* axis showing (*a*) electrostatic potential force, (*b*) dispersion force and (*c*) total energy. The radii of the cylinders are proportional to the relative magnitudes of the corresponding energies and were adjusted to the same scale factor of 55 with a cut-off value of 5 kJ mol^{-1} within 2 × 2 × 2 unit cells.

contacts and long-range H···H contacts. Whereas molecules between the supramolecular double layers are stabilized by long-range H···H contacts. Views of the energy framework diagrams down the *b* axis are shown in Fig. 7 and serve to emphasize the contribution of dispersion forces in the stabilization of the crystal.

7. Database survey

There are no close precedents for the substitution pattern observed in the tetra-substituted pyrrolidine ring of (II) with, arguably, the most closely related structure being that of (III) (KULQEP; Szcześniak *et al.*, 2015), at least in terms of the substitution pattern around the ring; the chemical diagram for (III) is shown in Fig. 8.

Table 4
Summary of interaction energies (kJ mol^{-1}) calculated for (II).

Contact	*R* (Å)	E_{ele}	E_{pol}	E_{dis}	E_{rep}	E_{tot}
Intra-double-layer						
C3—H3···O1^{ii} + C3—H3···O3^{ii} + O1···C10^{iv} + O5···C8^{ii}	6.8	−19.4	−8.3	−33.6	19.3	−44.0
H9*B*···H13*C*^{v} + H13*B*···H13*B*^{v}	8.2	−5.1	−1.6	−28.4	11.0	−24.5
C13—H13*A*···O5^{vi} + H4*B*···H11*C*^{vi} + H7*C*···H11*B*^{vi}	9.0	−8.8	−2.1	−20.8	10.7	−22.4
C11—H11*A*···O7^{iii} + C13—H13*C*···O4^{iii} + C10···O7^{vii}	7.9	−8.1	−2.9	−20.2	12.5	−20.6
H9*A*···H13*A*^{viii} + H9*C*···H9*C*^{viii}	9.3	−6.5	−2.1	−19.8	14.4	−16.7
C9—H9*B*···O5^{i}	9.1	−10.2	−2.3	−12.9	13.9	−15.1
C7—H7*B*···O7^{ix}	9.9	−3.6	−0.9	−15.1	4.8	−14.7
Inter-double-layer region						
H4*A*···H6*A*^{x} + H7*B*···H11*B*^{x}	8.1	−5.0	−1.8	−41.4	17.3	−31.9
H7*A*···H11*C*^{xi}	8.9	−0.9	−0.4	−10.8	6.2	−6.8

Symmetry codes: (i) −*x*, −*y*, −*z* + 2; (ii) *x* − 1, *y*, *z*; (iii) *x*, *y* − 1, *z*; (iv) *x* + 1, *y*, *z*; (v) −*x*, −*y* + 1, −*z* + 2; (vi) *x* + 1, *y* + 1, *z*; (vii) *x*, *y* + 1, *z*; (viii) −*x* + 1, −*y* + 1, −*z* + 2; (ix) −*x*, −*y* + 1, −*z*; (*x*) −*x*, −*y*, −*z* + 1; (xi) −*x* − 1, −*y*, −*z* + 1.

8. Synthesis and crystallization

A solution of (2*R*,3*S*,4*S*)-3,4-bis(acetyloxy)-1-(ethoxycarbonyl)pyrrolidine-2-carboxylic acid (40 mg, 0.132 mmol) in methanol (1 ml) was cooled to 273–278 K after which an excess of a cold, freshly prepared solution of CH_2N_2 in ether was added. The mixture was stirred at room temperature for 10 min. Excess CH_2N_2 was eliminated by purging the balloon with a dry air flow. The purge was collected on a solution of HOAc in MeOH. The reaction solution was concentrated to dryness and the residue was purified by flash column chromatography on silica gel, using a mixture of EtOAc/*n*-hexane (1:3). Yield: 41.7 mg (quantitative) of (II). Colourless irregular crystals for the X-ray analysis were obtained by the slow evaporation of its *n*-hexane solution. M.p. 347.6–348.7 K.

The ^{1}H and ^{13}C NMR reflect the presence of two conformational rotamers in solution. ^{1}H NMR (500 MHz, $CDCl_3$): δ = 5.38 (*s*, 1H, H_3); 5.11 (*s*, 1H, H_4); 4.51 and 4.42 (2*s*, 1H, H_2); 4.23–4.05 (2*m*, 2H, CH_2CH_3); 3.91 and 3.87 (2*dd*, *J* = 12.8 Hz and 5.5 Hz, 1H, H_{4a}); 3.772 and 3.766 (2*s*, 3H, CO_2CH_3); 3.63

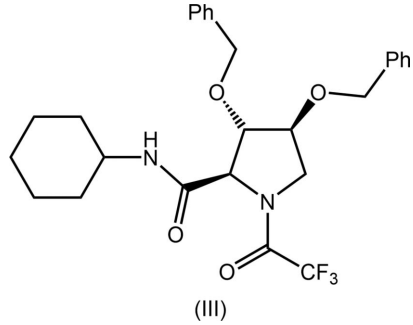

(III)

Figure 8
Chemical diagram for (III).

and 3.59 (2*d*, *J* = 12.8 Hz, 1H, H_{4b}); 2.10 and 2.09 (2*s*, 3H, Ac); 2.01 and 2.00 (2*s*, 3H, Ac); 1.28 and 1.21 (2*t*, *J* = 7.0 Hz, 3H, CH_2CH_3). ^{1}H NMR (500 MHz, C_6D_6, r.t.): δ = 5.62 (*s*, 1H, H_3); 5.07 and 5.02 (2*ap t*, *J* = 2.7 Hz, 1H, H_3); 4.78 (*s*, 0.6H, H_1); 4.55 (*s*, 0.4H, H_1); 4.12 and 4.10 (2*q*, *J* = 7.0 Hz, 0.4H, CH_2CH_3); 4.01–3.88 (*q* + *m*, *J* = 7.0 Hz, 2H, CH_2CH_3 and H_{4a}); 3.84–3.76 (*m*, 1H, H_{4b}); 3.65 (*dd*, *J* = 12.2 Hz and 2.4 Hz, 0.6H, H_{4a}); 3.31 and 3.30 (2*s*, 3H, CO_2CH_3); 1.48 and 1.45 (2*s*, 3H, Ac); 1.43 and 1.42 (2*s*, 3H, Ac); 0.94 and 0.92 (2*t*, *J* = 7.0 Hz, 3H, CH_2CH_3). ^{13}C NMR (125 MHz, $CDCl_3$, r.t.): δ = 169.4; 169.3; 169.2; 168.8; 168.7; 154.8; 154.4; 77.9; 76.9; 74.5; 73.5; 63.6; 63.5; 61.9; 61.7; 52.7; 52.6; 50.6; 50.4; 20.74; 20.70; 20.65; 14.5. Microanalysis calculated for $C_{13}H_{19}NO_8$: C 49.21, H 6.04, N 4.41%. Found: C 48.89, H 6.52, N 4.50%.

9. Refinement details

Crystal data, data collection and structure refinement details are summarized in Table 5. The carbon-bound H atoms were placed in calculated positions (C—H = 0.96–0.98 Å) and were included in the refinement in the riding-model approximation, with U_{iso}(H) set to 1.2–1.5U_{eq}(C).

Table 5
Experimental details.

Crystal data	
Chemical formula	$C_{13}H_{19}NO_8$
M_r	317.29
Crystal system, space group	Triclinic, $P\overline{1}$
Temperature (K)	290
a, *b*, *c* (Å)	6.8291 (5), 7.8670 (11), 15.814 (3)
α, β, γ (°)	100.607 (11), 99.011 (10), 105.054 (7)
V (Å^3)	787.5 (2)
Z	2
Radiation type	Mo *K*α
μ (mm^{-1})	0.11
Crystal size (mm)	0.40 × 0.35 × 0.10
Data collection	
Diffractometer	Enraf Nonius TurboCAD-4
No. of measured, independent and observed [$I > 2\sigma(I)$] reflections	4880, 4573, 2571
R_{int}	0.020
(sin $\theta/\lambda)_{max}$ (Å^{-1})	0.703
Refinement	
$R[F^2 > 2\sigma(F^2)]$, $wR(F^2)$, *S*	0.042, 0.128, 0.99
No. of reflections	4573
No. of parameters	203
H-atom treatment	H-atom parameters constrained
$\Delta\rho_{max}$, $\Delta\rho_{min}$ (e Å^{-3})	0.18, −0.17

Computer programs: *CAD-4 EXPRESS* (Enraf Nonius, 1989), *XCAD4* (Harms & Wocadlo, 1995), *SIR2014* (Burla *et al.*, 2015), *SHELXL2018/3* (Sheldrick, 2015), *ORTEP-3 for Windows* (Farrugia, 2012), *MarvinSketch* (ChemAxon, 2010), *DIAMOND* (Brandenburg, 2006) and *publCIF* (Westrip, 2010).

Funding information

The Brazilian agencies Coordination for the Improvement of Higher Education Personnel, CAPES, Finance Code 001 and the National Council for Scientific and Technological Development (CNPq) are acknowledged for grants (312210/2019–1, 433957/2018–2 and 406273/2015–4) to IC, for a fellowship (303207/2017–5) to JZS and a scholarship to SDP. Sunway University Sdn Bhd is also thanked for funding (grant. No. STR-RCTR-RCCM-001–2019).

References

Assefa, S. T., Yang, E.-Y., Chae, S.-Y., Song, M., Lee, J., Cho, M.-C. & Jang, S. (2020). *Plants*, **9** article No. 2.

Brandenburg, K. (2006). *DIAMOND*. Crystal Impact GbR, Bonn, Germany.

Brás, N. F., Cerqueira, N. M. F. S. A., Ramos, M. J. & Fernandes, P. A. (2014). *Expert Opin. Ther. Pat.* **24**, 857–874.

Burla, M. C., Caliandro, R., Carrozzini, B., Cascarano, G. L., Cuocci, C., Giacovazzo, C., Mallamo, M., Mazzone, A. & Polidori, G. (2015). *J. Appl. Cryst.* **48**, 306–309.

ChemAxon (2010). *MarvinSketch.* http://www.chemaxon.com.

Contreras-García, J., Johnson, E. R., Keinan, S., Chaudret, R., Piquemal, J.-P., Beratan, D. N. & Yang, W. (2011). *J. Chem. Theory Comput.* **7**, 625–632.

Dhameja, M. & Gupta, P. (2019). *Eur. J. Med. Chem.* **176** article No. 343e377.

Edwards, A. J., Mackenzie, C. F., Spackman, P. R., Jayatilaka, D. & Spackman, M. A. (2017). *Faraday Discuss.* **203**, 93–112.

Enraf Nonius (1989). *CAD-4 EXPRESS*. Enraf-Nonius, Delft, The Netherlands.

Farrugia, L. J. (2012). *J. Appl. Cryst.* **45**, 849–854.

Garcia, A. L. L. (2008). PhD thesis, Universidade Estadual de Campinas, UNICAMP, Campinas, SP, Brazil.

Harms, K. & Wocadlo, S. (1995). *XCAD4*. University of Marburg, Germany.

Johnson, E. R., Keinan, S., Mori-Sánchez, P., Contreras-García, J., Cohen, A. J. & Yang, W. (2010). *J. Am. Chem. Soc.* **132**, 6498–6506.

Kiappes, J. L., Hill, M. L., Alonzi, D. S., Miller, J. L., Iwaki, R., Sayce, A. C., Caputo, A. T., Kato, A. & Zitzmann, N. (2018). *Chem. Biol.* **13**, 60–65.

Liu, Z. & Ma, S. (2017). *ChemMedChem*, **12**, 819–829.

Matassini, C., Warren, J., Wang, B., Goti, A., Cardona, F., Morrone, A. & Bols, M. (2020). *Angew. Chem. Int. Ed.* **59** https://doi.org/10.1002/anie.202002850

McKinnon, J. J., Spackman, M. A. & Mitchell, A. S. (2004). *Acta Cryst.* B**60**, 627–668.

Sheldrick, G. M. (2015). *Acta Cryst.* C**71**, 3–8.

Spackman, M. A. & McKinnon, J. J. (2002). *CrystEngComm*, **4**, 378–392.

Spackman, M. A., McKinnon, J. J. & Jayatilaka, D. (2008). *CrystEngComm*, **10**, 377–388.

Spek, A. L. (2020). *Acta Cryst.* E**76**, 1–11.

Szcześniak, P., Maziarz, E., Stecko, S. & Furman, B. (2015). *J. Org. Chem.* **80**, 3621–3633.

Tan, S. L., Jotani, M. M. & Tiekink, E. R. T. (2019). *Acta Cryst.* E**75**, 308–318.

Turner, M. J., Mckinnon, J. J., Wolff, S. K., Grimwood, D. J., Spackman, P. R., Jayatilaka, D. & Spackman, M. A. (2017). *Crystal Explorer 17*. The University of Western Australia.

Westrip, S. P. (2010). *J. Appl. Cryst.* **43**, 920–925.

Zukerman-Schpector, J., Sugiyama, F. H., Garcia, A. L. L., Correia, C. R. D., Jotani, M. M. & Tiekink, E. R. T. (2017). *Acta Cryst.* E**73**, 1218–1222.

supporting information

Acta Cryst. (2020). E**76**, 967-972 [https://doi.org/10.1107/S205698902000701X]

1-Ethyl 2-methyl 3,4-bis(acetyloxy)pyrrolidine-1,2-dicarboxylate: crystal structure, Hirshfeld surface analysis and computational chemistry

Sofia Dallasta Pedroso, Ignez Caracelli, Julio Zukerman-Schpector, Monica Soto-Monsalve, Regina H. De Almeida Santos, Carlos Roque D. Correia, Ariel L. Llanes Garcia, Huey Chong Kwong and Edward R. T. Tiekink

Computing details

Data collection: *CAD-4 EXPRESS* (Enraf Nonius, 1989); cell refinement: *CAD-4 EXPRESS* (Enraf Nonius, 1989); data reduction: *XCAD4* (Harms & Wocadlo, 1995); program(s) used to solve structure: *SIR2014* (Burla *et al.*, 2015); program(s) used to refine structure: *SHELXL2018/3* (Sheldrick, 2015); molecular graphics: *ORTEP-3 for Windows* (Farrugia, 2012), *MarvinSketch* (ChemAxon, 2010) and *DIAMOND* (Brandenburg, 2006); software used to prepare material for publication: *publCIF* (Westrip, 2010).

1-Ethyl 2-methyl 3,4-bis(acetyloxy)pyrrolidine-1,2-dicarboxylate

Crystal data

$C_{13}H_{19}NO_8$
$M_r = 317.29$
Triclinic, $P\overline{1}$
$a = 6.8291$ (5) Å
$b = 7.8670$ (11) Å
$c = 15.814$ (3) Å
$\alpha = 100.607$ (11)°
$\beta = 99.011$ (10)°
$\gamma = 105.054$ (7)°
$V = 787.5$ (2) Å^3
$Z = 2$
$F(000) = 336$
$D_x = 1.338$ Mg m^{-3}
Mo $K\alpha$ radiation, $\lambda = 0.71073$ Å
Cell parameters from 25 reflections
$\theta = 10.8$–$18.2°$
$\mu = 0.11$ mm^{-1}
$T = 290$ K
Irregular, colourless
0.40 × 0.35 × 0.10 mm

Data collection

Enraf Nonius TurboCAD-4 diffractometer
Radiation source: Enraf Nonius FR590
non–profiled $\omega/2\theta$ scans
4880 measured reflections
4573 independent reflections
2571 reflections with $I > 2\sigma(I)$
$R_{int} = 0.020$
$\theta_{max} = 30.0°$, $\theta_{min} = 2.7°$
$h = -9\rightarrow9$
$k = 0\rightarrow11$
$l = -22\rightarrow21$
3 standard reflections every 120 min
intensity decay: 2%

Refinement

Refinement on F^2
Least-squares matrix: full
$R[F^2 > 2\sigma(F^2)] = 0.042$
$wR(F^2) = 0.128$
$S = 0.99$
4573 reflections
203 parameters
0 restraints
Primary atom site location: structure-invariant direct methods

Secondary atom site location: difference Fourier map	$w = 1/[\sigma^2(F_o^2) + (0.0579P)^2 + 0.0763P]$ where $P = (F_o^2 + 2F_c^2)/3$
Hydrogen site location: inferred from neighbouring sites	$(\Delta/\sigma)_{max} = 0.001$
H-atom parameters constrained	$\Delta\rho_{max} = 0.18$ e Å^{-3}
	$\Delta\rho_{min} = -0.17$ e Å^{-3}

Special details

Geometry. All esds (except the esd in the dihedral angle between two l.s. planes) are estimated using the full covariance matrix. The cell esds are taken into account individually in the estimation of esds in distances, angles and torsion angles; correlations between esds in cell parameters are only used when they are defined by crystal symmetry. An approximate (isotropic) treatment of cell esds is used for estimating esds involving l.s. planes.

Fractional atomic coordinates and isotropic or equivalent isotropic displacement parameters (Å²)

	x	*y*	*z*	U_{iso}*/U_{eq}
O1	0.28490 (19)	0.08131 (19)	0.64555 (9)	0.0568 (3)
O2	0.12213 (18)	0.24723 (18)	0.57354 (8)	0.0513 (3)
O3	0.35221 (19)	0.33818 (18)	0.83767 (9)	0.0586 (3)
O4	0.20434 (18)	0.14935 (17)	0.91551 (8)	0.0504 (3)
O5	−0.5275 (2)	−0.0729 (2)	0.83254 (9)	0.0662 (4)
O6	−0.32790 (16)	−0.06328 (15)	0.73314 (7)	0.0424 (3)
O7	−0.2014 (3)	0.6135 (2)	0.78612 (11)	0.0753 (4)
O8	−0.08692 (17)	0.40628 (15)	0.84074 (7)	0.0426 (3)
N1	0.0250 (2)	0.1764 (2)	0.69258 (9)	0.0433 (3)
C1	0.0322 (2)	0.0990 (2)	0.76913 (10)	0.0372 (3)
H1	0.041065	−0.024702	0.752792	0.045*
C2	−0.1782 (2)	0.0948 (2)	0.79177 (10)	0.0357 (3)
H2	−0.177363	0.096071	0.853908	0.043*
C3	−0.2178 (2)	0.2626 (2)	0.76694 (10)	0.0388 (3)
H3	−0.364464	0.257939	0.758613	0.047*
C4	−0.1353 (2)	0.2683 (2)	0.68313 (11)	0.0430 (4)
H4A	−0.244190	0.204920	0.631224	0.052*
H4B	−0.076679	0.392201	0.679209	0.052*
C5	0.1565 (2)	0.1615 (2)	0.63798 (10)	0.0424 (4)
C6	0.2518 (3)	0.2410 (3)	0.50973 (13)	0.0631 (5)
H6A	0.234590	0.116529	0.480776	0.076*
H6B	0.396809	0.298206	0.538377	0.076*
C7	0.1853 (4)	0.3399 (4)	0.44469 (15)	0.0818 (7)
H7A	0.041201	0.282919	0.417435	0.123*
H7B	0.266749	0.337723	0.400460	0.123*
H7C	0.204764	0.463198	0.474089	0.123*
C8	0.2155 (2)	0.2132 (2)	0.84352 (11)	0.0404 (3)
C9	0.3834 (3)	0.2283 (4)	0.98760 (14)	0.0766 (7)
H9A	0.506912	0.224946	0.966399	0.115*
H9B	0.370682	0.160845	1.032257	0.115*
H9C	0.391528	0.351722	1.012025	0.115*
C10	−0.4972 (2)	−0.1374 (2)	0.76304 (12)	0.0461 (4)
C11	−0.6347 (3)	−0.3050 (3)	0.69971 (16)	0.0697 (6)
H11A	−0.581462	−0.404559	0.706145	0.104*

H11B	−0.639848	−0.289168	0.640732	0.104*
H11C	−0.771979	−0.329842	0.711270	0.104*
C12	−0.0926 (3)	0.5768 (2)	0.84243 (13)	0.0500 (4)
C13	0.0585 (4)	0.7066 (3)	0.92107 (15)	0.0696 (6)
H13A	0.194942	0.735689	0.908739	0.104*
H13B	0.058933	0.652183	0.970653	0.104*
H13C	0.018502	0.815216	0.934292	0.104*

Atomic displacement parameters (Å²)

	U^{11}	U^{22}	U^{33}	U^{12}	U^{13}	U^{23}
O1	0.0482 (7)	0.0740 (9)	0.0610 (8)	0.0303 (7)	0.0206 (6)	0.0223 (7)
O2	0.0509 (7)	0.0668 (8)	0.0457 (6)	0.0205 (6)	0.0212 (5)	0.0231 (6)
O3	0.0431 (6)	0.0550 (8)	0.0714 (8)	0.0012 (6)	0.0106 (6)	0.0205 (7)
O4	0.0476 (6)	0.0545 (7)	0.0462 (6)	0.0117 (6)	0.0003 (5)	0.0186 (6)
O5	0.0573 (8)	0.0702 (10)	0.0703 (9)	0.0073 (7)	0.0301 (7)	0.0171 (8)
O6	0.0357 (5)	0.0405 (6)	0.0475 (6)	0.0065 (5)	0.0088 (5)	0.0092 (5)
O7	0.0854 (11)	0.0571 (9)	0.0929 (11)	0.0370 (8)	0.0070 (9)	0.0284 (8)
O8	0.0440 (6)	0.0367 (6)	0.0497 (6)	0.0151 (5)	0.0096 (5)	0.0122 (5)
N1	0.0395 (7)	0.0576 (9)	0.0448 (7)	0.0230 (6)	0.0144 (6)	0.0243 (6)
C1	0.0345 (7)	0.0403 (8)	0.0423 (8)	0.0148 (6)	0.0098 (6)	0.0168 (7)
C2	0.0327 (7)	0.0348 (8)	0.0397 (8)	0.0087 (6)	0.0082 (6)	0.0105 (6)
C3	0.0322 (7)	0.0404 (8)	0.0458 (8)	0.0125 (6)	0.0082 (6)	0.0127 (7)
C4	0.0411 (8)	0.0497 (10)	0.0446 (8)	0.0186 (7)	0.0094 (7)	0.0196 (7)
C5	0.0359 (7)	0.0520 (10)	0.0389 (8)	0.0111 (7)	0.0086 (6)	0.0118 (7)
C6	0.0635 (12)	0.0808 (15)	0.0527 (11)	0.0219 (11)	0.0292 (9)	0.0195 (10)
C7	0.0946 (17)	0.112 (2)	0.0566 (12)	0.0356 (15)	0.0357 (12)	0.0387 (13)
C8	0.0357 (7)	0.0424 (9)	0.0477 (9)	0.0155 (7)	0.0101 (6)	0.0154 (7)
C9	0.0645 (13)	0.0948 (18)	0.0570 (12)	0.0172 (12)	−0.0142 (10)	0.0169 (12)
C10	0.0358 (8)	0.0443 (9)	0.0596 (10)	0.0088 (7)	0.0106 (7)	0.0200 (8)
C11	0.0448 (10)	0.0558 (12)	0.0917 (16)	−0.0003 (9)	0.0043 (10)	0.0075 (11)
C12	0.0516 (9)	0.0402 (9)	0.0677 (12)	0.0181 (8)	0.0229 (9)	0.0213 (9)
C13	0.0803 (14)	0.0425 (11)	0.0764 (14)	0.0050 (10)	0.0192 (12)	0.0075 (10)

Geometric parameters (Å, º)

O1—C5	1.2098 (19)	C3—H3	0.9800
O2—C5	1.345 (2)	C4—H4A	0.9700
O2—C6	1.446 (2)	C4—H4B	0.9700
O3—C8	1.1961 (19)	C6—C7	1.484 (3)
O4—C8	1.3312 (19)	C6—H6A	0.9700
O4—C9	1.445 (2)	C6—H6B	0.9700
O5—C10	1.195 (2)	C7—H7A	0.9600
O6—C10	1.3499 (19)	C7—H7B	0.9600
O6—C2	1.4385 (18)	C7—H7C	0.9600
O7—C12	1.195 (2)	C9—H9A	0.9600
O8—C12	1.348 (2)	C9—H9B	0.9600
O8—C3	1.4496 (19)	C9—H9C	0.9600

N1—C5	1.351 (2)	C10—C11	1.483 (3)
N1—C1	1.4518 (19)	C11—H11A	0.9600
N1—C4	1.464 (2)	C11—H11B	0.9600
C1—C8	1.524 (2)	C11—H11C	0.9600
C1—C2	1.528 (2)	C12—C13	1.496 (3)
C1—H1	0.9800	C13—H13A	0.9600
C2—C3	1.521 (2)	C13—H13B	0.9600
C2—H2	0.9800	C13—H13C	0.9600
C3—C4	1.523 (2)		

C5—O2—C6	115.92 (14)	O2—C6—H6B	110.4
C8—O4—C9	115.73 (15)	C7—C6—H6B	110.4
C10—O6—C2	116.20 (12)	H6A—C6—H6B	108.6
C12—O8—C3	118.19 (13)	C6—C7—H7A	109.5
C5—N1—C1	121.34 (13)	C6—C7—H7B	109.5
C5—N1—C4	125.77 (13)	H7A—C7—H7B	109.5
C1—N1—C4	112.89 (12)	C6—C7—H7C	109.5
N1—C1—C8	111.47 (13)	H7A—C7—H7C	109.5
N1—C1—C2	102.32 (12)	H7B—C7—H7C	109.5
C8—C1—C2	113.23 (13)	O3—C8—O4	124.90 (16)
N1—C1—H1	109.9	O3—C8—C1	125.34 (15)
C8—C1—H1	109.9	O4—C8—C1	109.73 (13)
C2—C1—H1	109.9	O4—C9—H9A	109.5
O6—C2—C3	108.78 (12)	O4—C9—H9B	109.5
O6—C2—C1	106.68 (12)	H9A—C9—H9B	109.5
C3—C2—C1	103.23 (12)	O4—C9—H9C	109.5
O6—C2—H2	112.5	H9A—C9—H9C	109.5
C3—C2—H2	112.5	H9B—C9—H9C	109.5
C1—C2—H2	112.5	O5—C10—O6	122.72 (16)
O8—C3—C2	102.26 (11)	O5—C10—C11	125.62 (16)
O8—C3—C4	111.80 (12)	O6—C10—C11	111.66 (16)
C2—C3—C4	103.54 (13)	C10—C11—H11A	109.5
O8—C3—H3	112.8	C10—C11—H11B	109.5
C2—C3—H3	112.8	H11A—C11—H11B	109.5
C4—C3—H3	112.8	C10—C11—H11C	109.5
N1—C4—C3	103.35 (12)	H11A—C11—H11C	109.5
N1—C4—H4A	111.1	H11B—C11—H11C	109.5
C3—C4—H4A	111.1	O7—C12—O8	122.72 (18)
N1—C4—H4B	111.1	O7—C12—C13	126.78 (18)
C3—C4—H4B	111.1	O8—C12—C13	110.46 (16)
H4A—C4—H4B	109.1	C12—C13—H13A	109.5
O1—C5—O2	125.04 (15)	C12—C13—H13B	109.5
O1—C5—N1	124.93 (15)	H13A—C13—H13B	109.5
O2—C5—N1	110.02 (14)	C12—C13—H13C	109.5
O2—C6—C7	106.76 (17)	H13A—C13—H13C	109.5
O2—C6—H6A	110.4	H13B—C13—H13C	109.5
C7—C6—H6A	110.4		

C5—N1—C1—C8	76.02 (19)	C2—C3—C4—N1	−27.36 (15)
C4—N1—C1—C8	−103.88 (15)	C6—O2—C5—O1	−0.3 (3)
C5—N1—C1—C2	−162.67 (14)	C6—O2—C5—N1	−179.62 (15)
C4—N1—C1—C2	17.43 (18)	C1—N1—C5—O1	2.0 (3)
C10—O6—C2—C3	−96.72 (15)	C4—N1—C5—O1	−178.13 (17)
C10—O6—C2—C1	152.54 (13)	C1—N1—C5—O2	−178.67 (14)
N1—C1—C2—O6	80.73 (14)	C4—N1—C5—O2	1.2 (2)
C8—C1—C2—O6	−159.17 (12)	C5—O2—C6—C7	178.98 (17)
N1—C1—C2—C3	−33.83 (15)	C9—O4—C8—O3	−6.4 (3)
C8—C1—C2—C3	86.27 (14)	C9—O4—C8—C1	171.57 (15)
C12—O8—C3—C2	−176.59 (13)	N1—C1—C8—O3	−8.7 (2)
C12—O8—C3—C4	73.23 (17)	C2—C1—C8—O3	−123.40 (18)
O6—C2—C3—O8	168.91 (11)	N1—C1—C8—O4	173.33 (13)
C1—C2—C3—O8	−78.04 (13)	C2—C1—C8—O4	58.60 (17)
O6—C2—C3—C4	−74.78 (14)	C2—O6—C10—O5	3.0 (2)
C1—C2—C3—C4	38.26 (15)	C2—O6—C10—C11	−176.72 (15)
C5—N1—C4—C3	−173.74 (15)	C3—O8—C12—O7	0.4 (2)
C1—N1—C4—C3	6.15 (18)	C3—O8—C12—C13	−177.58 (14)
O8—C3—C4—N1	82.01 (15)		

Hydrogen-bond geometry (Å, º)

D—H···*A*	*D*—H	H···*A*	*D*···*A*	*D*—H···*A*
C9—H9*B*···O5^{i}	0.96	2.53	3.403 (3)	151
C3—H3···O1^{ii}	0.98	2.62	3.419 (2)	139
C3—H3···O3^{ii}	0.98	2.61	3.453 (2)	144
C11—H11*A*···O7^{iii}	0.96	2.66	3.329 (3)	127

Symmetry codes: (i) −*x*, −*y*, −*z*+2; (ii) *x*−1, *y*, *z*; (iii) *x*, *y*−1, *z*.